Nanoscale Research Letters

RESEARCH

Open Access

Synthesis of Novel Triphenylamine-Based Organic Dyes with Dual Anchors for Efficient Dye-Sensitized Solar Cells

Samar E. Mahmoud, Ahmed A. Fadda, Ehab Abdel-Latif and Mohamed R. Elmorsy*

Abstract

A new series of metal-free organic dyes (**SM1-5**) with dual anchors are synthesized for application in dye-sensitized solar cells (DSSC). Here, a simple triphenylamine (TPA) moiety serves as the electron donor, while di-cyanoacrylamide and di-thiazolidine-5-one units serve as the electron acceptors and anchoring groups. To understand the effect of dye structure on the photovoltaic characteristics of DSSCs, the photophysical and electrochemical properties, as well as molecular geometries calculated from density functional theory (DFT), are used for dyes **SM1-5**. The extinction coefficients of the organic dyes **SM1-5** are high (5.36–9.54 10^4 M^{-1} cm^{-1}), indicating a high aptitude for light harvesting. The photovoltaic studies indicated that using dye SM4 as a sensitizer showed a power conversion efficiency (PCE) of 6.09% (J_{SC} = 14.13 mA cm^{-2}, V_{OC} = 0.624 V, FF = 68.89%). Interestingly, **SM4** showed the highest values of V_{OC} among all dyes, including **N-719**, due to its maximum dye coverage on the TiO_2 surface, enhancing charge recombination resistance in the sensitized cell. The good agreement between the theoretically and experimentally obtained data indicates that the energy functional and basis set employed in this study can be successfully utilized to predict new photosensitizers' absorption spectra with great precision before synthesis. Also, these results show that bi-anchoring molecules have a lot of potentials to improve the overall performance of dye-sensitized solar cells.

Keywords: Di-cyanoacrylamide, Di-thiazolidine-5-one, Triphenylamine-based organic dyes, **N-719**

Background

Since the forerunner work on dye-sensitized solar cells (DSSCs) by Grätzel in 1991, DSSCs have received much research attention due to their enormous advantages such as low cost, good performance in low-light environments, high discipline, environmental friendliness and colors customizable [1, 2]. The power conversion efficiency of DSCs increased from 7% in 1991 to 14.3% in 2015 using liquid electrolytes (LEs), TiO_2 photoelectrode with nanoparticles sensitized with **ADEKA-1** and a carboxy-anchor organic dye, **LEG4** [3]. The details of the work of dye-sensitized solar cells were explained as reported [4, 5].

A DSSC consists of five major components: a semiconductor, a sensitizer, a counter electrode, a working electrode and an electrolyte [6, 7]. Semiconductors are ideal ingredients for DSSC anodes because of their large surface cross section area for photosensitizer anchoring. Photoanode materials include binary metal oxides such as TiO_2, SnO_2 and ZnO. In DSCs, TiO_2 is the most distinguished candidate for the photoanode. TiO_2 achieved high efficiencies due to its large band gap compared to traditional semiconductors and excellent physical properties such as chemical and optical stability and corrosion resistance [8, 9].

The counter electrode consists of a conducting layer on a plastic or glass substrate. Pt electrodes are commonly used due to their catalytic effect and high stability. Carbon black, silver and gold have also been tested as counter electrodes [10, 11].

*Correspondence: m.r.elmorsy@gmail.com

Department of Chemistry, Faculty of Science, Mansoura University, El-Gomhoria Street, Mansoura 35516, Egypt

The electrolyte is responsible for transporting charge between electrodes and continuously regenerates the dye during DSSC operation [12]. There are three types of electrolytes: liquid electrolytes, quasi-solid electrolytes and solid polymer electrolytes. The I_3^-/I^- redox couple was generally used in the electrolyte due to its high light absorption property and slow recombination reactions. Even though these liquid electrolytes lead to high efficiency, they cause problems such as leakage, being highly volatile, corrosion of metals and difficulties in the device sealing and fabrication processes. DSSCs based on a quasi-solid electrolyte can compete with liquid electrolytes in terms of PCE and exhibit better long-term stability. Solid-state conductors represent a strong solution to this shortage. Fenton and Wright proposed this type, which consists of complexes of alkali metal ions within a polymeric matrix. Park et al. added polar groups to the polymeric matrix to improve the ionic conductivity of solid polymer electrolytes [13–16].

The major patterns of photosensitizer are metal-free organic dyes [17]. Zeng et al. (2009) proposed that organic sensitizers containing triphenylamine units gave power conversion efficiencies of over 11% and 10% [18]. Yao et al. (2015) showed that the highest efficiency (η) of DSSCs employing a single metal-free organic dye has reached 13.0% and other dyes with PCE 11.8%. A rigidified phenanthrene-quinoxaline-based sensitizer was synthesized by Jiang et al. (2018), and the efficiency of its assembled DSSC reached 10.11% under AM1.5G irradiation [19, 20].

The chemical structure of the organic sensitizers plays an essential role in the features of photovoltaics in DSSCs [21]. One of the most important types of organic dyes is the conjugated donor–acceptor (D-π-A) because of its sturdy spectral response. The HOMO and LUMO levels of the sensitizers can be easily tuned by alternation of the donor, spacer, and acceptor moieties [22]. To increase the absorption of the metal-free organic dyes, many donor groups were introduced into structures such as triarylamine, carbazole, indole, coumarin and phenothiazine [23].

Triphenylamine units are more powerful electron donors than other substances, because of their fluorescence qualities and electron density. Furthermore, a well-known substance with a non-planar architecture that exhibits a stiff plane [24], three-dimensional steric, a hole transporting characteristic, light-harvesting features and decreased aggregation on semiconductor surfaces (TiO_2) [25]. To improve DSSC photovoltaic efficiency, photosensitizers are required to have bathochromic shifts by introducing donating groups (alkoxy, alkyl) and aromatic groups to TPA that increase the HOMO energy orbital level [26] or introducing different anchoring groups (CN, CO and NH) that facilitate the electron injection from the donor moiety into the photoanode and decrease charge aggregation of the dye on TiO_2 [27–32]. To improve the binding strength of dyes on TiO_2, the incorporation of double electron-accepting groups into the organic donor structure to generate a double-anchored compound has been suggested, which exhibited higher device efficiency than single D-π-A dyes [33–39].

We launched five new di-anchoring compounds with a triphenylamine core as an electron donor, denoted as **SM1-5**. In this work, we used different and new di-anchoring structures, which were created with three-electron acceptors (cyanoacrylamide core, thiazolidine-5-one-dimolononitrile core, and thiazolidine-5-one-bis(3-oxobutanoate core)). Using organic photosensitizers with double electron acceptors/anchoring groups led to improved current efficiency as a result of increasing the molar extinction coefficient of the chromophore and also led to improved photovoltage because of the absorption maximum amount of sensitizer on the semiconductor surface. The power conversion efficiency in the DSSC is better than the single electron acceptor type [40, 41]. Figure 1 displays the molecular structures of the components **SM1-5,** which were developed and produced. Figures 2, 3 and 4 illustrate the synthetic paths. The structure of dyes **SM1-5** is confirmed by FTIR, ^{1}H NMR, ^{13}C NMR and MS. Their optical properties were calculated from UV–Vis absorption. The electronic distribution of HOMO/LUMO energy levels was studied using Gaussian 09. Compared to the standard dye N-719 [42], their photovoltaic performance and electrochemical impedance spectroscopy (EIS) were also studied.

Experimental Section

Materials and Instruments

The solvents and chemicals used in the synthesis of sensitizers **SM1-5** were purchased from Sigma-Aldrich. The melting points (degrees centigrade) were obtained on the Gallenkamp electric melting point device. ^{1}H and ^{13}C NMR spectra were measured in DMSO-d_6 as a solvent at 500 MHz and 125 MHz, respectively, and obtained using JEOL's NMR spectrometer. The Nicolet iS10 FTIR spectrometer was used to measure IR spectra (KBr disks). The UV–Visible spectra were measured by using a UV–Vis spectrophotometer (T80 series). Thermo Scientific GC/MS model ISQ was used to determine mass analyses. Elemental analysis was recorded by a PerkinElmer 2400 analyzer. The CV experiments were conducted by following the three-electrode system, consisting of platinum as counter, Ag/AgCl as a reference electrode, and glassy carbon was used as the working electrode. The data were recorded at a scan rate of 100 mV^{-1}.

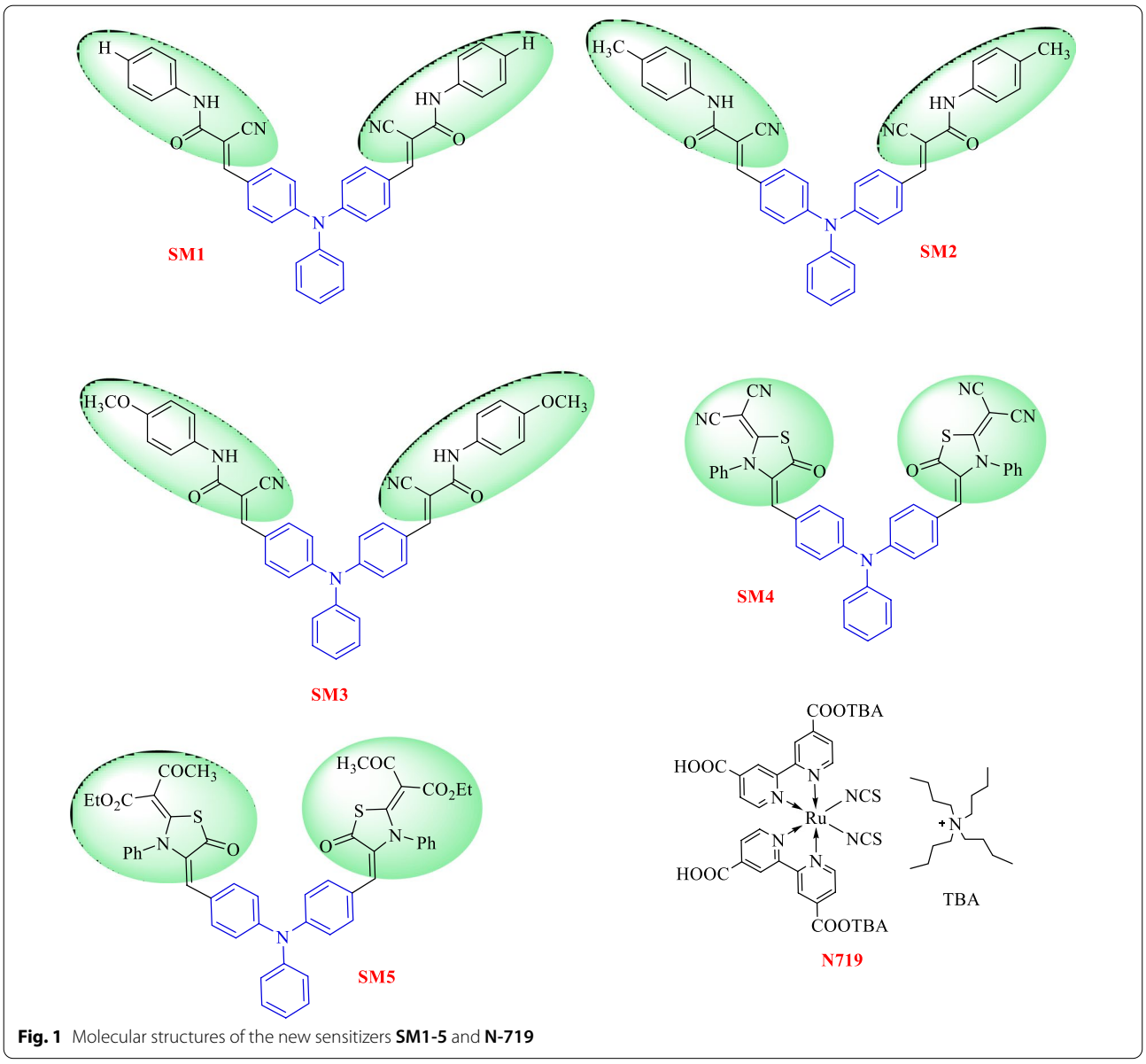

Fig. 1 Molecular structures of the new sensitizers **SM1-5** and **N-719**

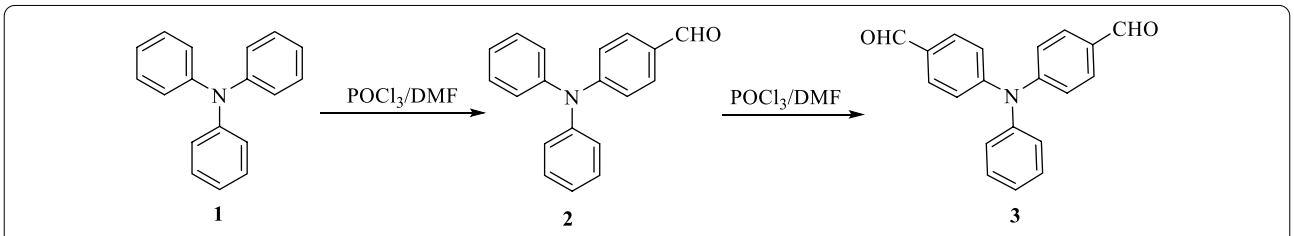

Fig. 2 Synthesis of 4,4′-diformyl-triphenylamine (**3**)

Photocurrent–voltage characteristics of DSSCs were measured using a Keithley 2400 source meter under illumination of AM 1.5 G solar light from a solar simulator (SOL3A, Oriel) equipped with a 450 W xenon lamp (91160, Oriel). The incident light intensity was calibrated using a reference Si solar cell (Newport Oriel, 91150 V)

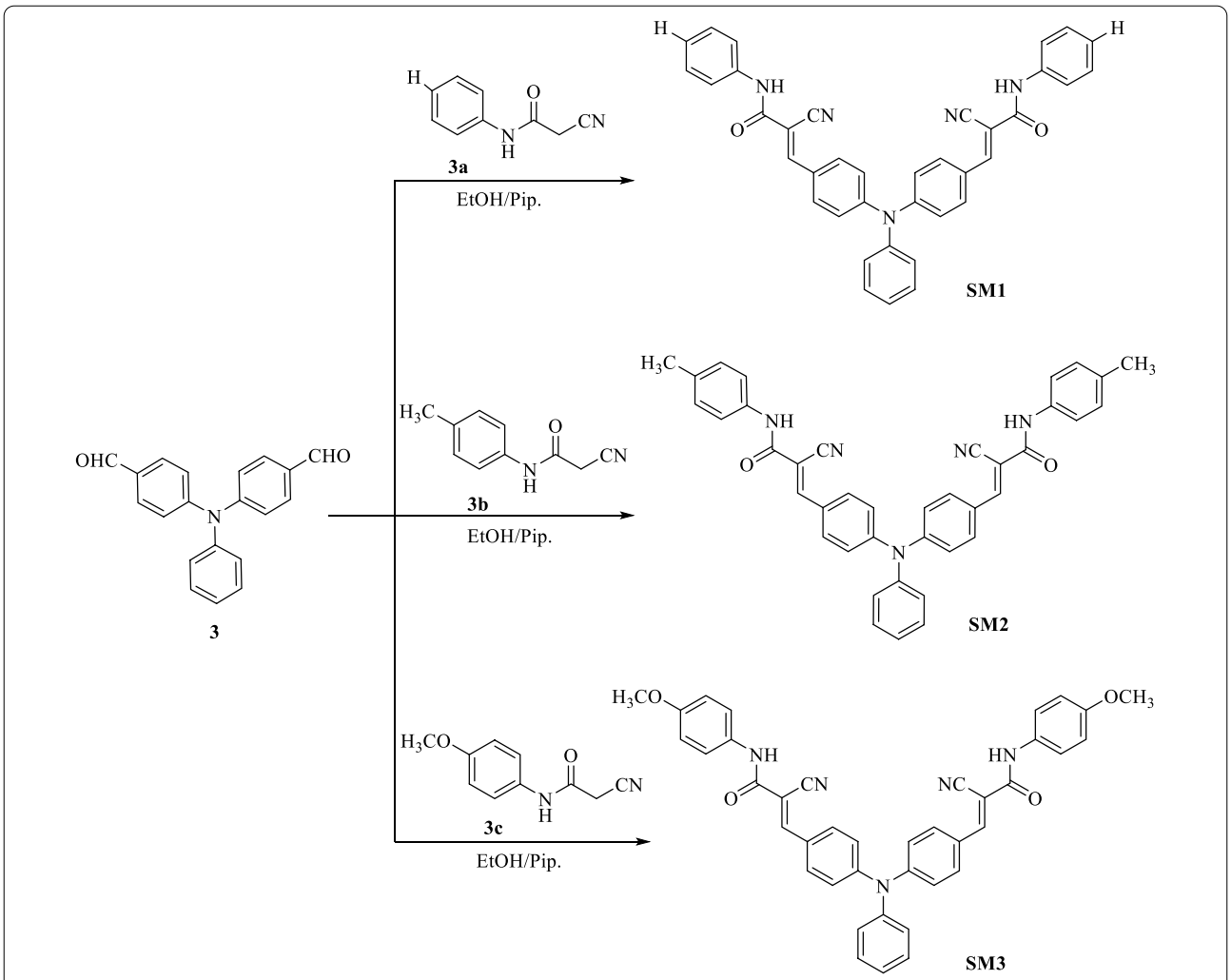

Fig. 3 Synthesis of 3,3′-((phenylimino)bis(4,1-phenylene))bis(*N*-aryl-cyanoacrylamide) sensitizers **SM1-3**

to set 1 Sun (100 mW cm^{-2}). The measurements were fully controlled under Oriel IV Test Station software. The electrochemical impedance spectra were measured with an impedance analyzer potentiostat (Bio-Logic SP-150) under illumination with a solar simulator (SOL3A, Oriel) equipped with a 450 W xenon lamp (91160, Oriel). EIS spectra were recorded over a frequency range of 100 mHz to 200 kHz at room temperature. The applied bias voltage was set at the *V*OC of the DSSCs with an AC amplitude of 10 mV. The electrical impedance spectra were fitted with Z-Fit software (Bio-Logic).

Synthesis of Targeted Sensitizers SM1-5

Synthesis of 4-(Diphenylamino)benzaldehyde (2)

The title compound **2** was synthesized in good yield by formylation of triphenylamine (**1**) according to the reported Vilsmeier–Haack reaction [43].

Synthesis of 4,4′-Diformyl-triphenylamine (3)

In a 50-mL two-neck RB flask containing dry DMF (23 mL, 300 mmol), freshly purified $POCl_3$ (24 mL, 260 mmol) was added dropwise at 0 °C, and the mixture was stirred in an argon atmosphere for 30 min at this temperature until the colored Vilsmeier salt completely precipitated. The solution of 4-(diphenylamino)benzaldehyde (**2**) (1 g, 4 mmol) dissolved in (10 mL) dry DMF was added, and the mixture of the reaction was stirred at 50 °C overnight. The mixture was cooled at room temperature, poured into ice water and neutralized to pH 7 with sodium acetate. The crude product was purified by

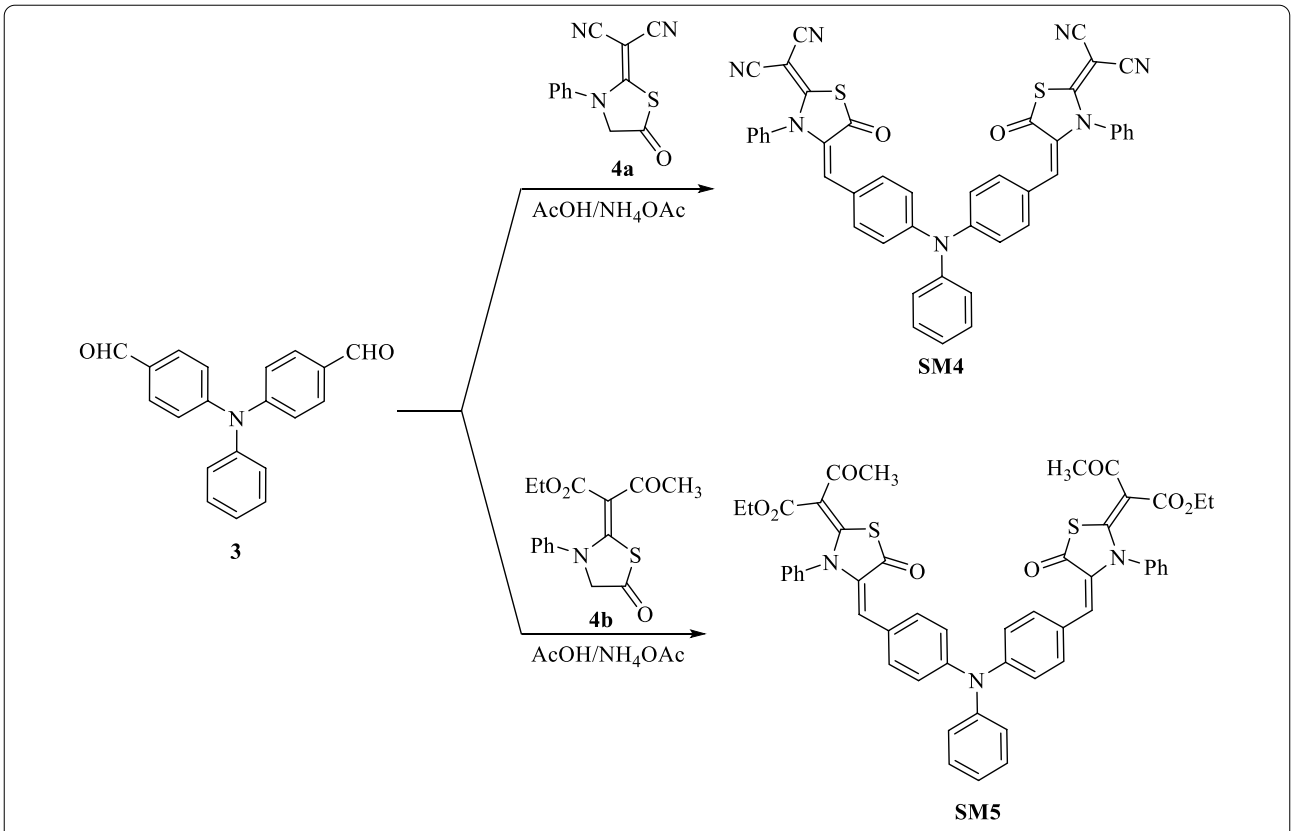

Fig. 4 Synthesis of triphenylamine-thiazolidine-5-one sensitizers **SM4** and **SM5**

column chromatography using the mixture of SiO_2 and CH_2Cl_2 to produce yellow crystals.

90% yield; m.p. = 142–144 °C, lit. m.p. = 141–143 °C [43]. IR ($\bar{\upsilon}$, cm^{-1}): 1691 (2 C=O). ^1H NMR (δ/ppm): 7.16–7.19 (m, 7H, Ar–H), 7.39 (t, 2H, Ar–H), 7.77 (d, 4H, Ar–H), 9.8 (s, 2H, 2 CH=O). Analysis for $C_{20}H_{15}NO_2$ (301.11): calculated: C, 79.72; H, 5.02; N, 4.65%, found: C, 79.55; H, 5.08; N, 4.74%.

General Synthesis of 3,3′-((Phenylimino)bis(4,1-phenylene))bis(*N*-aryl-cyanoacrylamide) Sensitizers SM1-3

In a dry 50-mL RB flask, 4 mmol of each cyanoacetanilide derivative **3a–c** (namely 2-cyanoacetanilide (0.64 g, 4 mmol), 2-cyano-*p*-methylacetanilide (0.70 g, 4 mmol) and 2-cyano-*p*-methoxyacetanilide (0.76 g, 4 mmol)) was added to a solution of 4,4'-diformyl-triphenylamine (**3**) (0.60 g, 2 mmol) in 50 mL dry ethanol and 0.1 mL piperidine. The mixture was subjected to heating for 2 h. The crystalline finished product on hot was collected, rinsed with hot EtOH and refined by recrystallization to provide the sensitizers **SM1**, **SM2** and **SM3**, respectively.

3′-((Phenylimino)bis(4,1-phenylene))bis(2-cyano-N-phenylacrylamide) (SM1)

Orange powder; 79% yield; m.p. = 265–266 °C. IR ($\bar{\upsilon}$, cm^{-1}): 3332 (2 N–H), 2210 (2 C≡N), 1679 (2 C=O). ^1H NMR (δ/ppm): 7.12 (t, 2H, Ar–H), 7.19 (d, 4H, Ar–H), 7.24 (d, 2H, Ar–H), 7.31–7.37 (m, 5H, Ar–H), 7.48 (t, 2H, Ar–H), 7.65 (d, 4H, Ar–H), 7.98 (d, 4H, Ar–H), 8.19 (s, 2H, 2 CH = C), 10.29 (s, 2H, 2 N–H). ^{13}C NMR (δ/ppm): 104.09 (2C), 116.78 (2C), 120.63 (4C), 122.26, 122.59 (2C), 122.80, 124.30 (2C), 126.18 (2C), 126.48, 127.13 (2C), 128.77 (4C), 130.43 (2C), 131.38, 132.21 (2C), 138.35 (2C), 144.90, 149.64 (2C), 149.83 (2C), 151.36, 160.86 (2C). Mass analysis (*m*/*z*, %): 585 (M^+, 24.27), 427 (42.52), 346 (58.22), 295 (30.47), 265 (27.16), 157 (54.05), 117 (37.70), 92 (83.55), 79 (27.02). Analysis for $C_{38}H_{27}N_5O_2$ (585.22), calculated: C, 77.93; H, 4.65; N, 11.96%, found: C, 77.79; H, 4.70; N, 11.87%.

3′-((Phenylimino)bis(4,1-phenylene))bis(2-cyano-N-(p-tolyl) acrylamide) (SM2)

Orange powder; 76% yield; m.p. above 300 °C. IR ($\bar{\upsilon}$, cm^{-1}): 3380 (2 N–H), 2208 (2 C≡N), 1689 (2 C=O). ^1H NMR (δ/ppm): 2.27 (s, 6H, 2 CH_3) 7.14–7.25 (m, 10H, Ar–H), 7.32 (t, 1H, Ar–H), 7.46 (q, 2H, Ar–H), 7.53 (d,

4H, Ar–H), 7.96 (d, 4H, Ar–H), 8.17 (s, 2H, 2 CH=C), 10.19 (s, 2H, 2 N–H). ^{13}C NMR (δ/ppm): 21.03 (2C), 105.10 (2C), 114.08 (4C), 116.88 (2C), 121.98 (2C), 122.38 (4C), 122.98 (2C), 123.17, 125.24 (2C), 126.34, 127.15 (2C), 130.11 (2C), 131.05 (2C), 132.37 (2C), 145.95 (2C), 149.76 (2C), 149.98 (2C), 155.94 (2C), 161.03 (2C). Mass analysis (*m*/*z*, %): 613 (M^+, 10.42), 581 (18.24), 403 (21.88), 303 (34.30), 286 (44.03), 282 (99.22), 188 (40.58), 82 (58.71), 60 (62.61), 41 (67.21), 40 (100.00). Analysis for $C_{40}H_{31}N_5O_2$ (613.25): calculated: C, 78.28; H, 5.09; N, 11.41%, found: C, 78.38; H, 5.05; N, 11.33%.

3′-((Phenylimino)bis(4,1-phenylene))bis(2-cyano-N-(4-methoxyphenyl)acrylamide) (SM3)

Dark orange powder; 74% yield; m.p.=274–276 °C. IR ($\bar{\upsilon}$, cm^{-1}): 3360 (2 N–H), 2206 (2 C≡N), 1680 (2 C=O). ^{1}H NMR (δ/ppm): 3.73 (s, 6H, 2 OCH_3), 6.92 (d, 4H, Ar–H), 7.18 (d, 4H, Ar–H), 7.23 (d, 2H, Ar–H), 7.31 (t, 1H, Ar–H), 7.48 (t, 2H, Ar–H), 7.55 (d, 4H, Ar–H), 7.96 (d, 4H, Ar–H), 8.16 (s, 2H, 2 CH=C), 10.15 (s, 2H, 2 N–H). ^{13}C NMR (δ/ppm): 55.21 (2C), 104.10 (2C), 113.86 (4C), 116.84 (2C), 122.18, 122.33 (4C), 122.58 (3C), 122.87, 126.24 (2C), 126.44, 127.10 (2C), 130.41 (2C), 131.31 (2C), 132.15 (3C), 144.93, 149.55 (2C), 149.58 (2C), 155.97 (2C), 160.42 (2C). Mass analysis (*m*/*z*, %): 645 (M^+, 41.66), 566 (46.65), 529 (58.87), 518 (63.83), 508 (73.91), 458 (100.00), 381 (61.55), 347 (48.00), 298 (86.32), 250 (59.37), 237 (48.43), 188 (83.61), 178 (95.65), 160 (90.38), 131 (62.40), 118 (87.81), 102 (49.64), 67 (41.52). Analysis for $C_{40}H_{31}N_5O_4$ (645.24): calculated: C, 74.40; H, 4.84; N, 10.85%, found: C, 74.58; H, 4.76; N, 10.97%.

General Synthesis of Triphenylamine-thiazolidine-5-one Sensitizers SM4 and SM5

In a dry 50-mL RB flask, 4 mmol of each thiazolidine-5-one derivative **4a** or **4b** [namely, 2-(5-oxo-3-phenylthiazolidine-2-ylidene) malononitrile (0.96 g, 4 mmol), ethyl-3-oxo-2-(5-oxo-3-phenylthiazolidine-2-ylidene) butaneperoxoate (1.22 g, 4 mmol)] was added to a mixture of 4,4′-diformyl-triphenylamine (**3**) (0.60 g, 2 mmol) and ammonium acetate (0.39 g, 5 mmol) in 30 ml of glacial acetic acid. The mixture was subjected to reflux for 2 h. The collected precipitate was purified and dried to **SM4** and **SM5**, respectively.

2′-((((Phenylimino)bis(4,1-phenylene))bis(methanylylidene))bis(5-oxo-3phenylthiazolidine-4,2-diylidene))dimalononitrile (SM4)

Red powder; 85% yield; m.p.=259–260 °C. IR ($\bar{\upsilon}$, cm^{-1}): 2215 (2 C≡N), 1721 (2 C=O). ^{1}H NMR (δ/ppm): 7.20 -7.26 (m, 6H, Ar–H), 7.32 (q, 1H, Ar–H), 7.48 (q, 2H, Ar–H), 7.56 -7.60 (m, 10H, Ar–H), 7.71 (d, 4H, Ar–H), 8.00 (s, 2H, 2 CH=C). ^{13}C NMR (δ/ppm): 110.00, 114.05, 115.03 (2C), 122.13, 122.96 (3C), 123.31, 126.72 (2C), 127.17 (2C), 127.23 (2C), 129.31 (4C), 129.60 (4C), 130.45 (2C), 131.29, 131.37, 132.55 (3C), 133.27 (2C), 134.93 (2C), 144.99, 148.62 (2C), 162.34, 165.97 (2C), 167.13 (2C), 191.22, 191.46. Mass analysis (*m*/*z*, %): 747 (M^+, 14.99), 710 (34.96), 675 (40.09), 594 (29.54), 461 (50.93), 356 (65.05), 347 (40.19), 225 (27.23), 175 (34.60), 64 (54.51), 62 (57.61), 51 (62.00), 44 (100.00), 43 (97.07). Analysis for $C_{44}H_{25}N_7O_2S_2$ (747.15): calculated: C, 70.67; H, 3.37; N, 13.11%, found: C, 70.98; H, 3.45; N, 13.26%.

Diethyl 2,2′-((((phenylimino)bis(4,1-phenylene))bis(methanylylidene))bis(5-oxo-3-phenylthiazolidine-4,2-diylidene))-bis(3-oxobutanoate) (SM5)

Red powder; 87% yield; m.p.=255–256 °C. IR ($\bar{\upsilon}$, cm^{-1}): 1709 (2 C=O), 1644 (2 C=O). ^{1}H NMR (δ/ppm): 1.03 (t, J=7.50 Hz, 6H, 2 CH_3), 2.08 (s, 6H, 2 $COCH_3$), 4.27 (q, 4H, 2 CH_2), 7.21 (d, 6H, Ar–H), 7.28 (t, 1H, Ar–H), 7.34 (d, 4H, Ar–H), 7.44–7.52 (m, 8H, Ar–H), 7.69 (d, 4H, Ar–H), 7.73 (s, 2H, 2 CH=C). ^{13}C NMR (δ/ppm): 14.00 (2C), 29.90 (2C), 62.09 (2C), 110.14, 114.96 (2C), 116.26 (2C), 122.21, 122.97 (4C), 123.56, 125.93 (2C), 126.58 (2C), 127.31 (2C), 129.29 (4C), 130.10 (4C), 131.55, 132.48 (2C), 133.51 (2C), 135.00 (2C), 146.05, 148.26 (2C), 149.35, 152.16, 162.83, 166.15 (2C), 167.98 (2C), 192.30 (2C). Mass analysis (*m*/*z*, %): 876 (M^+, 30.24), 849 (39.53), 777 (30.21), 655 (26.12), 640 (26.12), 507 (26.51), 476 (29.77), 376 (31.21), 372 (60.01), 269 (47.79), 216 (27.95), 151 (26.25), 148 (40.27), 91 (60.27). Analysis for $C_{50}H_{41}N_3O_8S_2$ (875.23): calculated: C, 68.56; H, 4.72; N, 4.80%, found: C, 68.79; H, 4.62; N, 4.91%.

Results and Discussion

Synthesis and Structure Characterization of Sensitizers SM1-5

The synthetic routes for the 3,3′-((phenylimino) bis(4,1-phenylene)) bis(*N*-aryl-cyanoacrylamide) sensitizers **SM1-3** are depicted in Figs. 2 and 3. Ren et al. were able to monoformylate triphenylamine (**1**) to make 4-(diphenylamino)benzaldehyde (**2**) [43]. According to the reported procedure [44], 4-(diphenylamino)benzaldehyde (**2**) then goes through another formylation to prepare 4,4′-diformyl-triphenylamine (**3**).

Finally, Knoevenagel condensation reaction of 4,4′-diformyl-triphenylamine (**3**) with cyanoacetanilide derivatives **3a-c** in dry ethanol and drops of piperidine as a catalyst furnished the targeted 3,3′-((phenylimino) bis(4,1-phenylene))bis(*N*-aryl-cyanoacrylamide) sensitizers **SM1-3** with yields of 79%, 76% and 74%. The cyanoacetylation of aniline, *p*-toluidine and *p*-anisidine with 1-cyanoacetyl-3,5-dimethylpyrazole in boiling dioxane was used to make the cyanoacetanilide derivatives **3a–c** [45].

The structures of these sensitizers are confirmed by elemental and spectroscopic analyses (IR, ^{1}H NMR, ^{13}C NMR and MS). The chemical structure of dye **SM1** was confirmed by characteristic absorption bands from the IR spectrum: N–H groups at 3332 cm^{-1}; cyano groups (C≡N) at 2210 cm^{-1}; and a broad absorption band for the carbonyl groups (C=O) at 1679 cm^{-1}. Its ^{1}H NMR spectrum showed a singlet for two olefinic protons at δ 8.19 ppm and a singlet at δ 10.29 ppm for two protons of two N–H groups. The aromatic protons resonate as doublet, triplet and multiplet signals in the region from δ 7.12 to 7.98 ppm. Its ^{13}C NMR spectrum exhibited the characteristic carbon signals at δ 116.78 ppm for (2C≡N), δ 149.83 ppm for (2C=C) and δ 160.86 ppm for (2C=O).

Also, the IR spectrum of **SM2** exhibited absorption bands at 3380 cm^{-1}, 2208 cm^{-1} and 1689 cm^{-1} for the N–H, C≡N and C=O functional groups. Its ^{1}H NMR spectrum showed singlet for six protons at 2.27 ppm is distinct for two methyl groups, a singlet for two olefinic protons and two protons of N–H groups at δ 8.17 and 10.19 ppm, respectively. Its mass spectrum displayed a molecular ion peak at $m/z = 613$, corresponding to the general formula $C_{40}H_{31}N_5O_2$. The structure of **SM3** was proved from the IR spectrum that showed three characteristic absorption bands at 3360 cm^{-1}, 2206 cm^{-1} and 1680 cm^{-1} for N–H, C≡N and C=O groups, respectively. The ^{1}H NMR spectrum showed a singlet at δ 3.73 ppm for six protons that is assignable to methoxy groups, singlet for two olefinic protons at δ 8.16 ppm and two protons of N–H groups at δ 10.15 ppm. Its ^{13}C NMR spectrum showed signals for two similar carbons of methoxy, nitrile and carbonyl groups at δ 55.21, 116.84 and 160.42 ppm, respectively. It had a molecular ion peak at $m/z = 645$, which corresponded to a molecular formula of $C_{40}H_{31}N_5O_4$.

The synthetic pathway of triphenylamine-thiazolidine-5-one dyes **SM4** and **SM5** is displayed in Fig. 4 according to the Knoevenagel condensation reaction between each thiazolidine-5-one derivative **4a** or **4b** [46] and 4,4'-diformyl-triphenylamine (**3**). The reaction proceeds by heating in acetic acid containing ammonium acetate to furnish the targeted dyes **SM4** and **SM5** in high yields of 85% and 87%, respectively. The chemical structure of organic synthesizers was identified by performing various spectra data. The IR spectrum of dye **SM4** exhibited a broad absorption at 2215 cm^{-1} and 1721 cm^{-1} for (C≡N) and (C=O) groups. Its ^{1}H NMR spectrum showed a singlet at δ 8.00 ppm for the olefinic protons. Its ^{13}C NMR spectrum showed signals of two analogical carbons of (C≡N) at δ 115.03 ppm and two signals of (C=O) at δ 191.22 and 191.46 ppm, respectively. Its mass spectrum exhibited a molecular ion peak at $m/z = 747$, which corresponds to the molecular formula $C_{44}H_{25}N_7O_2S_2$. Further, the IR spectrum of **SM5** displayed the characteristic absorption of two carbonyl groups at 1709 and 1644 cm^{-1}. Its ^{1}H NMR spectrum showed two singlet signals of methyl and olefinic protons at δ 2.08 and 7.73 ppm, a triplet at δ 1.03 for six protons (two methyl groups) and a quartet for four protons at δ 4.27 ppm (two methylene groups). Its mass spectrum showed that the molecular ion peak was at $m/z = 876$, which is the same as $C_{50}H_{41}N_3O_8S_2$ as a molecular formula.

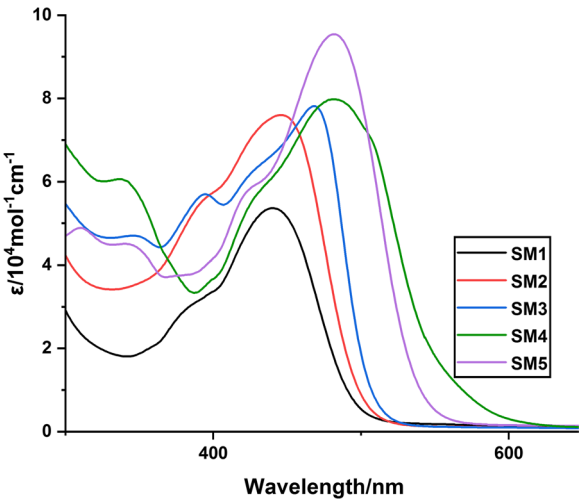

Fig. 5 UV–Vis absorption spectra of **SM1-5**measured in DMF (2×10^{-5} M)

Table 1 Absorption data for sensitizers **SM1-5**

Sensitizer	Absorption λ_{max} (nm)	ε (10^4 M^{-1} cm^{-1})	λ_{onset} (nm)	Practical $E_{0\text{-}0}$ (eV)
SM1	375, 441	2.69, 5.36	494	2.50
SM2	389, 446	5.58, 7.60	508	2.44
SM3	393, 470	5.68, 7.75	514	2.41
SM4	424, 483	5.73, 7.98	553	2.24
SM5	419, 483	5.57, 9.54	543	2.28

Optical Behavior and Electrochemical Properties of Dyes

The UV–Vis absorption spectra of five new organic sensitizers **SM1-5** in dimethylformamide (DMF) solution with a concentration (2×10^{-5} M) are recorded in Fig. 5. Table 1 contains typical spectral data. All dyes possess different absorption bands; the region with a lower wavelength (300–430 nm) is assigned to the π–π* transitions, and another region with a longer wavelength (440–560 nm) is due to intramolecular (ICT) from an arylamine donating moiety (triphenylamine)

to an electron acceptor (cyanoacrylamide moiety and thiazolidine-5-one derivatives). The maximum absorption wavelengths of five dyes **SM1-5** are 441 nm (molar extinction coefficient/$\varepsilon = 5.36 \times 10^4$ M^{-1} cm^{-1}), 446 nm (molar extinction coefficient/$\varepsilon = 7.60 \times 10^4$ M^{-1} cm^{-1}), 470 nm (molar extinction coefficient/$\varepsilon = 7.75 \times 10^4$ M^{-1} cm^{-1}) and 483 nm (molar extinction coefficient/$\varepsilon = 7.9 8 \times 10^4$ M^{-1} cm^{-1}), 483 nm (molar extinction coefficient /$\varepsilon = 9.54 \times 10^4$ M^{-1} cm^{-1}). Further, the onset of the highest absorption band wavelength (λ_{onset}) of the UV–visible spectra can also be used to compute $E_{0\text{-}0}$ (energy gap) [47]. $E_{0\text{-}0}$ values for compounds **SM1-5** are 2.50, 2.44, 2.41, 2.24 and 2.28 eV, respectively.

From Table 1, **SM4** and **SM5**, which have the thiazolidine-5-one moiety, exhibited bathochromic shift and lower energy compared to cyanoacrylamide units. This bathochromic shift provides good indication for gathering photons from the solar light, which results in better photovoltaic performance. Furthermore, the molar extinction coefficients of the absorption maximum wavelength are substantially bigger than for the other components **SM1-3**, indicating a strong aptitude for light harvesting. The lowest energy gap of **SM4** is attributed to the lower resonance energy, high conjugation system and presence of an electron-withdrawing group (CN) attached to the thiazolidine moiety as an anchor, which facilitates the charge transfer. On the other hand, **SM3**, which has cyanoacrylamide, appeared to have a bathochromic shift compared to cyanoacrylamides (**SM1** and **SM2**) due to the strong electron-donating group (methoxy group). The lack of a substituent on the phenyl group of the cyanoacrylmide is what makes **SM**1 bad at absorbing things.

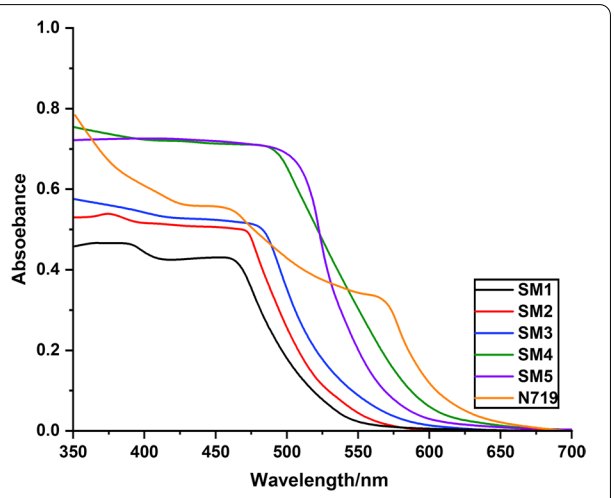

Fig. 6 UV–Vis spectra of **SM1-5** and **N-719** adsorbed on TiO_2 films

The normalized spectral data for the five components of TiO_2 particles are shown in Fig. 6. The absorption bands of the five structures on TiO_2 particle surfaces were redshifted relative to the spectra in the DMF solution. That may be related to the significant interactions among different components and the TiO_2 particles, particularly the creation of *J*-type aggregation. Additionally, as compared to **SM2-5** dye, **SM1** dye has a higher, redshifted merit, suggesting that **SM1** has a higher ability to cluster on TiO_2. Interestingly, the absorption spectra of **SM4** on the TiO_2 surface are identical with those of the dye in solution, demonstrating that the dye does not aggregate.

Cyclic voltammetry (CV) measurements were performed in DMF solution to estimate the thermodynamic probability of electron injection and dye regeneration. Ferrocene (0.4 V vs. normal hydrogen electrode (NHE)) is served as an external reference to regulate the redox potential. Additional file 1: Fig. 23 is the cyclic voltammetry curves of **SM1-5**. The corresponding data are displayed in Table 2. The ground state oxidation potential (GSOP) levels for **SM1-5** were generally considered acceptable and higher than the iodine/triiodide redox overall value (−5.2 eV), which confirmed that there is enough thermodynamic driving force to regenerate the dye by replenishing the hole through electron donation from the I_3^-/I^- redox couple. Moreover, the estimated excited state potentials (ESOP) for **SM1-5**, computed from GSOP - $E_{0\text{-}0}$, are −3.36 eV, −3.31 eV, −3.27 eV, -−3.16 eV and −3.21 eV, respectively.

The ESOP values of structures **SM1-5** are clearly above the conduction band (CB) of TiO_2 (−4.2 eV). This means

Table 2 Electrochemical data for dyes **SM1-5**

Dye	Practical parameters (eV)			Calculated parameters (eV)		
	$E_{0\text{-}0}$	HOMO	LUMO	$E_{0\text{-}0}$	HOMO	LUMO
SM1	2.50	−5.86	−3.36	2.64	−5.89	−3.25
SM2	2.44	−5.75	−3.31	2.69	−5.87	−3.18
SM3	2.41	−5.68	−3.27	2.58	−5.73	−3.15
SM4	2.24	−5.40	−3.16	2.36	−5.35	−2.99
SM5	2.28	−5.49	−3.21	2.39	−5.43	−3.04

that it is thermodynamically spontaneous for an electron to move from the excited state of the dyes into the CB of TiO_2. Furthermore, **SM4** has a more negative free energy of electron injection than other dyes, which indicates that the light-excited electrons are injected more efficiently in the case of **SM4**. These results indicate that these compounds have the prerequisites to be employed as dye-sensitized solar cells. The energy level diagram of dyes **SM1-5** is shown in Fig. 7.

Theoretical Investigation

The metal-free dyes **SM1-5** were optimized using DFT simulations with the Gaussian 09 software [48, 49] to explore their molecular geometry and electron circulation. The computations were carried out using the B3LYP exchange correlation functional using the basis set 6-311G (d, P) [50, 51]. Figure 8 depicts the optimized structures and molecular orbital distributions of **SM1-5**. As shown in Fig. 8, the electron distribution of the highest occupied molecular orbital (HOMO) for **SM1-5** may be detected across the molecules, notably in conjugated systems, while at the lowest unoccupied molecular orbital (LUMO), the distribution of the electrons for the five dyes is located over the acceptor moieties, especially on the cyanoacrylamides to **SM1-3** and over the thiazolidine-5-one moiety to **SM4** and **SM5**. This leads to a greater electronic coupling between the excited electrons of the dye in the LUMO and the unfilled *d*-orbitals of the semiconductor.

Photovoltaic Performances of DSSCs

Under the illumination of AM 1.5G solar light from a solar simulator (SOL3A, Oriel), the photovoltaic results of DSSCs designed and manufactured utilizing **SM1-5** and the benchmark dye **N-719** on the TiO_2 anode material using 10 mM chenodeoxycholic acid (CDCA) as a co-adsorbent were investigated using a Keithley 2400 source meter. The DSSC devices were fabricated according to the technique outlined in the Additional file 1 [52–54] with the goal of confirming the structure–performance assembly for compounds **SM1-5**. Furthermore, the co-adsorbent CDCA works as a proton buffer for the sensitizers, regulating dye proton concentration and so permitting enhanced dye adsorption on the anode nanoparticles [55, 56]. It also aids in the suppression of dye accumulation and covering of the TiO_2 surface, resulting in a reduction in the redox electrolyte's electron recombination process. The presence of new acceptor segments in the chemical modification of **SM1-5** has had a significant impact on photovoltaic parameters like open-circuit photovoltage (V_{OC}), short-circuit photocurrent density (J_{SC}), fill factor (FF) and overall solar light to electricity conversion efficiency (η) of the sensitized cells in the proposed investigation. The current–voltage (J–V) characteristics curves of the DSSCs made with **SM1-5** are shown in Fig. 9, and the results are summarized in Table 3.

The photovoltaic efficiency of the fabricated cells was found to be as follows: **SM4** > **SM5** > **SM3** > **SM2** > **SM1**. It is also important to mention that the thiazolidine-5-one **SM4** and **SM5** showcased higher performance than the cyanoacrylamides **SM1-3**. The highest performance

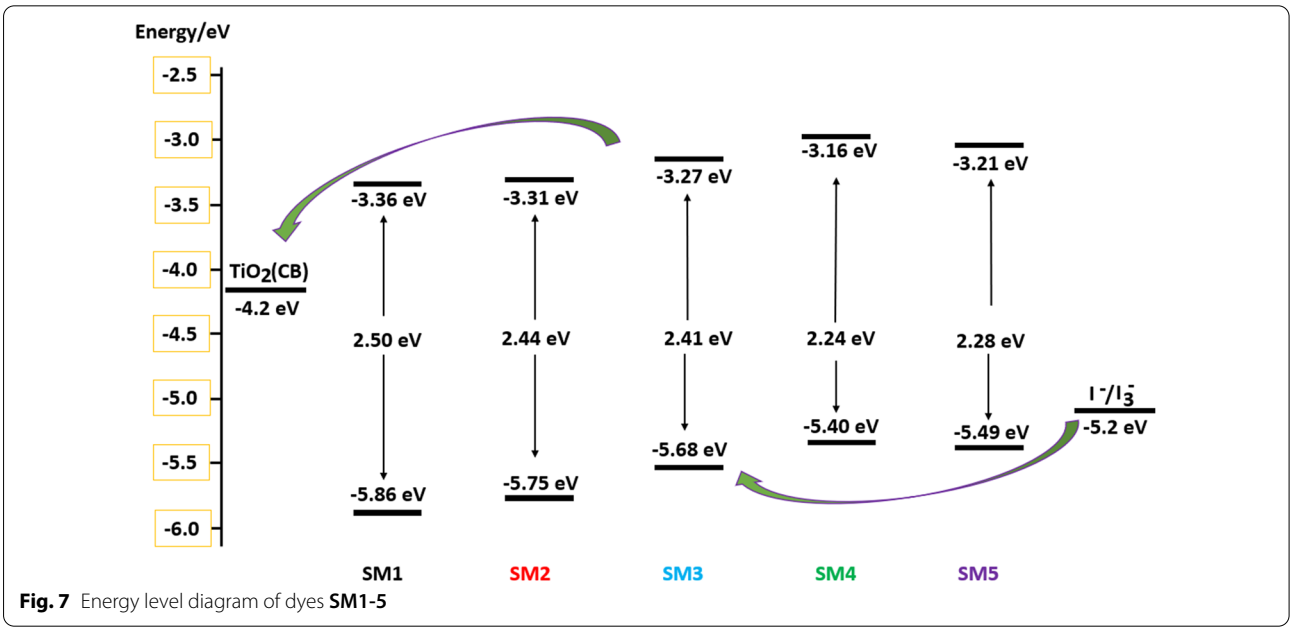

Fig. 7 Energy level diagram of dyes **SM1-5**

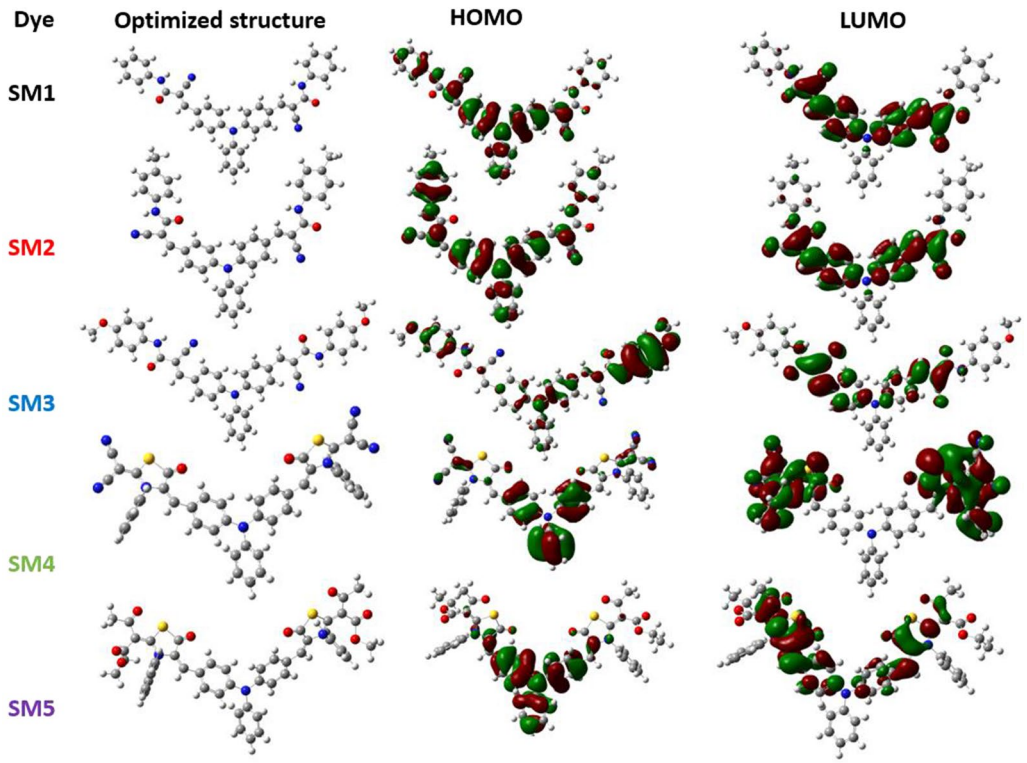

Fig. 8 Optimized structures and molecular orbital distributions of SM1-5

was achieved using **SM4** as follows: $\eta = (6.09\%)$, superior J_{SC} (14.13 mA cm^{-2}), and the greatest photovoltage value (0.624 V). The **SM1**, **SM2**, **SM3** and **SM5** fabricated devices showed η values of 1.33%, 2.34%, 3.52% and 5.34%, respectively. The higher performance of thiazildine-5-one dyes (**SM4**, **5**) compared to cyanoacrylamide dyes (**SM1-3**) is attributed to the maximum values of the J_{SC} and V_{OC}. The remarkably enhanced J_{SC} related to their higher dye loading than the cyanoacetamide-based dyes **SM1-3**. Generally, dye loading studies are performed in the quest to understand the difference in efficiency with the variation in the anchoring groups. Keeping this in view, to estimate the total amount of dye adsorbed on the TiO_2 surface, desorption of the dye from the TiO_2 was done using 0.1 M NaOH in DMF/H_2O (1:1) mixture. The obtained data are summarized in Table 3. From the results, it is quite evident that concentration of **SM4** on TiO_2 surface was higher than that of other four dyes. This is in agreement with the experimentally obtained J_{SC} values of **SM4**, which is the highest among the three sensitizers.

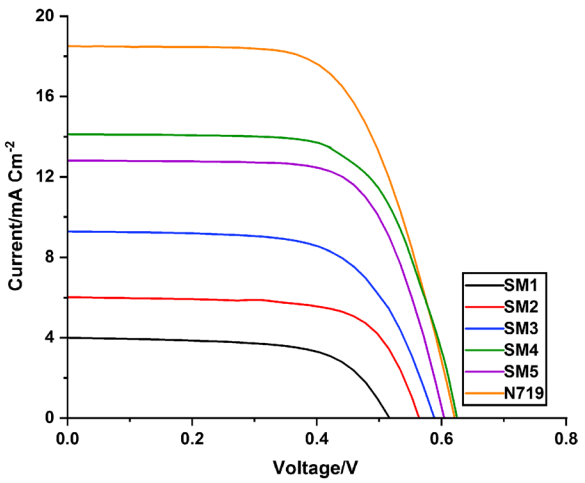

Fig. 9 *J–V* characteristics curves of the DSSCs fabricated using **SM1-5** and **N719**

Interestingly, **SM4** showed the highest values of V_{OC} among all dyes, including **N-719**. Due to the site-selective adsorption behavior of the **SM4**, the adsorption of prepared **SM4** may form a better dye coverage to help to passivate the TiO_2 surface or form an insulating molecular layer composed of prepared dye and thus reduces the recombination due to electron back-transfer between TiO_2 and I_3^-/I^-. Also, the **SM4** can be adsorbed on the TiO_2 surface with a higher density than the **N-719**

Table 3 *J–V* parameters of **SM1-5** and **N-719**

Dye	V_{OC}[a] (V_{OC}[b]) (V)	J_{SC}[a] (J_{SC}[b]) (mA cm^{-2})	FF[a] (FF[b]) (%)	η[a] (η[b]) (%)	Dye loading (mol cm^{-2})
SM1	**0.515** (0.498 ± 0.017)	**4.06** (3.94 ± 0.12)	**63.81** (63.5 ± 0.31)	**1.33** (1.24 ± 0.09)	**2.19** × 10^{-8}
SM2	**0.563** (0.538 ± 0.022)	**6.06** (5.84 ± 0.22)	**68.53** (68.35 ± 0.18)	**2.34** (2.15 ± 0.19)	**4.15** × 10^{-8}
SM3	**0.587** (0.572 ± 0.015)	**9.3** (9.17 ± 0.13)	**64.37** (64.06 ± 0.31)	**3.52** (3.36 ± 0.16)	**5.14** × 10^{-8}
SM4	**0.624** (0.614 ± 0.009)	**14.13** (14.06 ± 0.06)	**68.89** (68.55 ± 0.33)	**6.09** (5.91 ± 0.18)	**4.21** × 10^{-7}
SM5	**0.602** (0.581 ± 0.018)	**12.83** (12.54 ± 0.29)	**68.95** (68.55 ± 0.39)	**5.34** (4.89 ± 0.44)	**3.87** × 10^{-7}
N719	**0.620** (0.605 ± 0.049)	**18.51** (18.34 ± 0.38)	**63.47** (63.21 ± 0.26)	**7.3** (7.01 ± 0.28)	**1.65** × 10^{-6}

V_{OC}: the open circuit voltage, J_{SC}: the short current density, *FF*: the fill factor, and η: the efficiency

[a] The best device parameters (listed in the manuscript)

[b] The average device parameters (obtained from four devices)

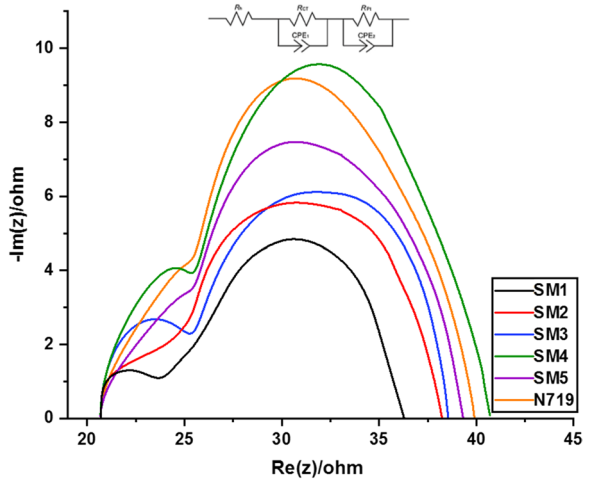

Fig. 10 Nyquist plots of SM1-5- and N-719-based devices

because it has multiple-anchoring groups. This finding clearly shows that the thiazolidine-5-one unit can potentially serve as an efficient electron-accepting platform or metal-free dye in order to increase device performance.

EIS Studies

Electrochemical impedance spectroscopy (EIS) is a powerful technique used to estimate the charge recombination in DSSCs [57, 58]. Figure 10 shows the Nyquist plots of the fabricated dyes **SM1-5** along with standard **N-719** and their equivalent circuit (inset Fig. 9). The EIS spectrum of a cell exhibited two semicircles in the Nyquist plots. Generally, the first semicircle at high frequencies represents the redox charge transfer resistances at the Pt/electrolyte interface (R_{pt}). The second semicircle at higher frequencies is related to the charge transfer resistances at the interface between TiO_2/dye/electrolyte (R_{CT}). Usually, a larger R_{CT} value indicates an increased charge recombination resistance and therefore a larger open-circuit photovoltage [58, 59].

The charge recombination resistance of these dyes (R_{CT}) corresponding to the diameter of the middle-frequency semicircle was calculated to decrease in the order **SM4** (20.32 Ω), **N-719** (18.13 Ω), **SM5** (16.05 Ω), **SM3** (15.12 Ω), **SM2** (14.17 Ω) and **SM1** (12.26 Ω), in good agreement with the order photovoltage data. The result indicates that dye **SM4** with thiazolidine-5-one can more effectively reduce charge recombination at the TiO_2/dye/electrolyte interface than other dyes and **N-719** dye. These results were also consistent with the V_{OC} of the DSSCs.

Conclusion

In conclusion, five new di-anchored metal-free organic dyes **SM1-5** were effectively developed, produced, and characterized. Optoelectronic, electrochemical, and molecular modeling studies show that structures **SM1-5** meet all the requirements for acting as photosensitizers. Additionally, theoretical investigations on compounds **SM1-5** show that the electron density shifts significantly from the triphenylamine donor to the acceptor/anchoring group through the π-spacer. The device fabricated with the **SM4** sensitizer displayed the highest photon to current efficiency (PCE of 6.09%). Its J_{SC} and V_{OC} were 14.13 mA cm^{-2} and 0.624 V, respectively. The inclusion of a strongly electron-withdrawing dimalononitrile unit on each side of the thiazolidine-5-one core accounts for

its improved performance. The findings clearly imply that the thiazolidine-5-one unit connected to the malononitrile core might be an outstanding electron acceptor system for metal-free dyes in order to increase power conversion efficiency. Molecular engineering is being used to develop DSSCs with organic dye-sensitized solar cells depending on the framework of **SM4**, with the goal of improving solar performance.

Supplementary Information

The online version contains supplementary material available at https://doi.org/10.1186/s11671-022-03711-6.

Additional file 1. Supplementary figures.

Acknowledgements
Not applicable.

Author Contributions
SEM contributed to synthesis, methodology and graphical plots. AAF and EA-L helped in supervision, initial corrections and comments. MRE performed synthesis, writing original draft, data analysis, editing, proofreading and manuscript handling. All authors read and approved the final manuscript.

Funding
Open access funding provided by The Science, Technology & Innovation Funding Authority (STDF) in cooperation with The Egyptian Knowledge Bank (EKB). Open access funding is provided by The Science, Technology & Innovation Funding Authority (STDF) in cooperation with The Egyptian Knowledge Bank (EKB). Further, the authors are thankful to Mansoura University, Egypt, for their support under project ID: MU-SCI-21-19.

Availability of Data and Materials
All data supporting the conclusions of this article are included within the article and supplementary document.

Declarations

Ethics Approval and Consent to Participate
Not applicable.

Consent for Publication
Not applicable.

Competing interests
The authors declare no competing interests.

Received: 4 June 2022 Accepted: 31 July 2022
Published online: 04 August 2022

References

1. Peter LM (2011) The gratzel cell: where next? J Phys Chem Lett 2(15):1861–1867. https://doi.org/10.1021/jz200668q
2. Lim DS, Choi K, Hayati D, Park DH, Ghifari A, Lee KM, Ko Y, Jun Y, Suk HJ, Hong J (2020) Blue-colored dyes featuring a diketopyrrolopyrrole spacer for translucent dye-sensitized solar cells. Dyes Pigments 173:107840. https://doi.org/10.1016/j.dyepig.2019.107840
3. Kakiage K, Aoyama Y, Yano T, Oya K, Fujisawa JI, Hanaya M (2015) Highly efficient dye-sensitized solar cells with collaborative sensitization by silyl-anchor and carboxy-anchor dyes. Chem Commun 51(88):15894–15897. https://doi.org/10.1039/C5CC06759F
4. Ardo S, Meyer GJ (2009) Photodriven heterogeneous charge transfer with transition-metal compounds anchored to TiO_2 semiconductor surfaces. Chem Soc Rev 38(1):115–164. https://doi.org/10.1039/b804321n
5. Fagiolari L, Varaia E, Mariotti N, Bonomo M, Barolo C, Bella F (2021) Poly(3,4-ethylenedioxythiophene) in dye-sensitized solar cells: toward solid-state and platinum-free photovoltaics. Adv Sustain Syst 5(11):2100025. https://doi.org/10.1002/adsu.202100025
6. Yen YS, Hsu JL, Ni JS, Lin JT (2021) Influence of various dithienoheterocycles as conjugated linker in naphtho [2,3-d][1,2,3] triazole-based organic dyes for dye-sensitized solar cells. Dyes Pigments 188:109220. https://doi.org/10.1016/j.dyepig.2021.109220
7. Sharma K, Sharma V, Sharma SS (2018) Dye-sensitized solar cells: fundamentals and current status. Nanoscale Res Lett 13(1):1–46. https://doi.org/10.1186/s11671-018-2760-6
8. Wu H, Zhang D, Lei BX, Liu ZQ (2022) Metal oxide based photoelectrodes in photoelectrocatalysis: advances and challenges. ChemPlusChem 87(5):e202200097. https://doi.org/10.1002/cplu.202200097
9. Brella M, Taabouche A, Gharbi B, Gheriani R, Bouachiba Y, Bouabellou A, Serrar H, Touil S, Laggoune K, Boudissa M (2022) Comparison of thin films of titanium dioxide deposited by sputtering and sol-gel mthods for waveguiding applications. Semiconductors 56(3):234–239. https://doi.org/10.1134/S106378262106004X
10. Yadav SC, Sharma A, Devan RS, Shirage PM (2022) Role of different counter electrodes on performance of TiO_2 based dye-sensitized solar cell (DSSC) fabricated with dye extracted from hibiscus sabdariffa as sensitizer. Opt Mater 124:112066. https://doi.org/10.1016/j.optmat.2022.112066
11. Liu S, Qi W, Cao Y, Liang C, Geng S, Guo H, Liu Y, Luo Y, Zhang W, Li L (2022) Design and characterization of frog egg shaped CoFe2O4@C core-shell composite as a novel multi-functional counter electrode for low-cost energy devices. J Alloys Compd 915:165395. https://doi.org/10.1016/j.jallcom.2022.165395
12. De Haro JC, Tatsi E, Fagiolari L, Bonomo M, Barolo C, Turri S, Bella F, Griffini G (2021) Lignin-based polymer electrolyte membranes for sustainable aqueous dye-sensitized solar cells. ACS Sustain Chem Eng 9(25):8550–8560. https://doi.org/10.1021/acssuschemeng.1c01882
13. Venkatesan S, Hsu TH, Wong XW, Teng H, Lee YL (2022) Tandem dye-sensitized solar cells with efficiencies surpassing 33% under dim-light conditions. Chem Eng J 2:137349. https://doi.org/10.1016/j.cej.2022.137349
14. Li J, Liu C, Miao C, Kou Z, Xiao W (2022) Enhanced ionic conductivity and electrochemical stability of Indium doping $Li_{1.3}Al_{0.3}Ti_{17}(PO_4)_3$ solid electrolytes for all-solid-state lithium-ion batteries. Ionics 28(1):63–72. https://doi.org/10.1007/s11581-021-04310-8
15. Galliano S, Bella F, Bonomo M, Giordano F, Grätzel M, Viscardi G, Hagfeldt A, Gerbaldi C, Barolo C (2021) Xanthan-based hydrogel for stable and efficient quasi-solid truly aqueous dye-sensitized solar cell with cobalt mediator. Sol RRL 5(7):2000823. https://doi.org/10.1002/solr.202000823
16. Rahman NA, Hanifah SA, Mobarak NN, Ahmad A, Ludin NA, Bella F, Su'ait MS (2021) Chitosan as a paradigm for biopolymer electrolytes in solid-state dye-sensitised solar cells. Polymer 230:124092. https://doi.org/10.1016/j.polymer.2021.124092
17. Akula SB, Tingare YS, Su C, Chen HS, Li WQ, Lekphet W, Li WR (2021) Bridgehead nitrogen tripodal organic dyes having multiple donor-π-acceptor branches for solar cell applications. Dyes Pigments 186:108985. https://doi.org/10.1016/j.dyepig.2020.108985
18. Zeng W, Cao Y, Bai Y, Wang Y, Shi Y, Zhang M, Wang F, Pan C, Wang P (2010) Efficient dye-sensitized solar cells with an organic photosensitizer featuring orderly conjugated ethylenedioxythiophene and dithienosilole blocks. Chem Mater 22(5):1915–1925. https://doi.org/10.1021/cm9036988
19. Su R, Lyu L, Elmorsy MR, El-Shafei A (2019) Novel metal-free organic dyes constructed with the DD|A-π-A motif: sensitization and co-sensitization study. Sol Energy 194:400–414. https://doi.org/10.1016/j.solener.2019.10.061
20. Yao Z, Wu H, Li Y, Wang J, Zhang J, Zhang M, Guo Y, Wang P (2015) Dithienopicenocarbazole as the kernel module of low-energy-gap organic dyes for efficient conversion of sunlight to electricity Energy. Environ Sci 8(11):3192–3197. https://doi.org/10.1039/c5ee02822a

21. Obotowo IN, Obot IB, Ekpe UJ (2016) Organic sensitizers for dye-sensitized solar cell (DSSC): properties from computation, progress and future perspectives. J Mol Struct 1122:80–87. https://doi.org/10.1016/j.molstruc.2016.05.080
22. Wu G, Kaneko R, Islam A, Zhang Y, Sugawa K, Han L, Shen Q, Bedja I, Gupta RK, Otsuki J (2016) Thiocyanate-free asymmetric ruthenium (II) dye sensitizers containing azole chromophores with near-IR light-harvesting capacity. J Power Source 331:100–111. https://doi.org/10.1016/j.jpowsour.2016.09.040
23. Han L, Chen Q, Yu H, Lu Y, Jiang S (2021) Triphenylamine dyes bearing 4-phenyl-2-(thiophen-2-yl) thiazole bridge for dye sensitized solar cells. Photochem Photobiol A 416:113341. https://doi.org/10.1016/j.jphotochem.2021.113341
24. Balasaravanan R, Duraimurugan K, Sivamani J, Thiagarajan V, Siva A (2015) Synthesis and photophysical properties of triphenylamine-based multiply conjugated star-like molecules. New J Chem 39(9):7472–7480. https://doi.org/10.1039/c5nj00605h
25. Sambathkumar S, Priyadharshini S, Fleisch M, Bahnemann DW, Kumar GG, Senthilarasu S, Renganathan R (2019) Design and synthesis of imidazole-triphenylamine based organic materials for dye sensitized solar cells. Mater Lett 242:28–31. https://doi.org/10.1016/j.matlet.2019.01.091
26. Hagberg DP, Yum JH, Lee H, De Angelis F, Marinado T, Karlsson KM, Humphry-Baker R, Sun L, Hagfeldt A, Grätzel M, Nazeeruddin MK (2008) Molecular engineering of organic sensitizers for dye-sensitized solar cell applications. J Am Chem Soc 130(19):6259–6266. https://doi.org/10.1021/ja800066y
27. Chen YH, Nguyen VS, Chou HH, Tingare YS, Wei TC, Yeh CY (2020) Anthracene organic sensitizer with dual anchors for efficient and robust dye-sensitized solar cells. ACS Appl Energy Mater 3(6):5479–5486. https://doi.org/10.1021/acsaem.0c00464
28. Elmorsy MR, Lyu L, Abdel-Latif E, Badawy S, El-Shafei AM, Fadda A (2020) Co-sensitization of HD-2 complex with low-cost cyanoacetanilides for highly efficient DSSCs. Photochem Photobiol Sci 19(2):281–288. https://doi.org/10.1039/c9pp00381a
29. Eltoukhi M, Fadda A, Abdel-Latif E, Elmorsy M (2022) Low cost carbazole-based organic dye bearing the acrylamides and 2-pyridone moieties for efficient dye-sensitized solar cells. J Photochem Photobiol A Chem 426:113760. https://doi.org/10.1016/j.jphotochem.2021.113760
30. Elmorsy M, Abdel-Latif E, Badawy S, Fadda A (2020) New cyanoacetanilides based dyes as effective co-sensitizers for DSSCs sensitized with ruthenium(II) complex (HD-2). J Mater Sci Mater Electron 31(10):7981–7990. https://doi.org/10.1007/s10854-020-03337-3
31. Badawy S, Su R, Fadda A, Abdel-Latif E, El-Shafei A, Elmorsy M (2021) Highly efficient (*N*-benzothiazolyl)-cyanoacetamide based co-sensitizers for high efficiency dye-sensitized solar cells. Optik 249:168274. https://doi.org/10.1016/j.ijleo.2021.168274
32. Alnakeeb A, Fadda A, Ismail M, Elmorsy M (2022) Efficient co-sensitization of novel trimethoxybenzene-based dyes with N-719 for highly efficient dye-sensitized solar cells. Opt Mater 128:112344. https://doi.org/10.1016/j.optmat.2022.112344
33. Grisorio R, De Marco L, Allegretta G, Giannuzzi R, Suranna GP, Manca M, Mastrorilli P, Gigli G (2013) Anchoring stability and photovoltaic properties of new D(-π-A)$_2$ dyes for dye-sensitized solar cell applications. Dyes Pigments 98(2):221–231. https://doi.org/10.1016/j.dyepig.2013.02.012
34. Abbotto A, Manfredi N, Marinzi C, De Angelis F, Mosconi E, Yum JH, Xianxi Z, Nazeeruddin MK, Grätzel M (2009) Dibranched di-anchoring organic dyes for dye-sensitized solar cells. Energy Environ Sci 2(10):1094–1101. https://doi.org/10.1039/b910654e
35. Hong Y, Liao JY, Fu JL, Kuang DB, Meier H, Su CY, Cao D (2012) Performance of dyesensitized solar cells based on novel sensitizers bearing asymmetric double D-π-A chains with arylamines as donors. Dyes Pigments 94(3):481–489. https://doi.org/10.1016/j.dyepig.2012.02.011
36. Seo KD, You BS, Choi IT, Ju MJ, You M, Kang HS, Kim HK (2013) Dual-channel anchorable organic dyes with well-defined structures for highly efficient dye-sensitized solar cells. J Mater Chem A 1(34):9947–9953. https://doi.org/10.1039/c3ta11832k
37. Ren X, Jiang S, Cha M, Zhou G, Wang ZS (2012) Thiophene-bridged double D-π-A dye for efficient dye-sensitized solar cell. Chem Mater 24(17):3493–3499. https://doi.org/10.1021/cm302250y
38. Sirohi R, Kim DH, Yu S-C, Lee SH (2012) Novel di-anchoring dye for DSSC by bridging of two mono anchoring dye molecules: a conformational approach to reduce aggregation. Dyes Pigments 92(3):1132–1137. https://doi.org/10.1016/j.dyepig.2011.09.003
39. Li Q, Shi J, Li H, Li S, Zhong C, Guo F, Peng M, Hua J, Qin J, Li Z (2012) Novel pyrrole-based dyes for dye-sensitized solar cells: from rod-shape to "H" type. J Mater 22(14):6689–6696. https://doi.org/10.1039/c2jm30200d
40. Beni AS, Hosseinzadeh B, Azari M, Ghahary R (2017) Synthesis and characterization of new triphenylamine-based dyes with novel anchoring groups for dye-sensitized solar cell applications. J Mater Sci Mater Electron 28(2):1859–1868. https://doi.org/10.1007/s10854-016-5737-1
41. Jo HJ, Choi YC, Ryu JH, Kang JH, Park NK, Lee DK, Kim JH (2010) Synthesis and characterization of organic photo-sensitizers containing multi-acceptors for the application of dye-sensitized solar cells. Mol Cryst Liq Cryst 532(1):55–471. https://doi.org/10.1080/15421406.2010.497115
42. Nazeeruddin M, Zakeeruddin M, Humphry-Baker R, Jirousek M, Liska P, Vlachopoulos N, Grätzel M (1999) Acid-Base equilibria of (2,2′-Bipyridyl-4,4′-dicarboxylic acid) ruthenium(II) complexes and the effect of protonation on charge-transfer sensitization of nanocrystalline titania. Inorg Chem 38(26):6298–6305. https://doi.org/10.1021/ic990916a
43. Ren W, Zhuang H, Bao Q, Miao S, Li H, Lu J, Wang L (2014) Enhancing the coplanarity of the donor moiety in a donor-acceptor molecule to improve the efficiency of switching phenomenon for flash memory devices. Dyes Pigments 100:127–134. https://doi.org/10.1016/j.dyepig.2013.09.002
44. Hosseinzadeh B, Beni AS, Azari M, Zarandi M, Karami M (2016) Novel D-π-A type triphenylamine based chromogens for DSSC: design, synthesis and performance studies. New J Chem 40(10):8371–8381. https://doi.org/10.1039/c6nj01314g
45. Fadda AA, Bondock S, Rabie R, Etman HA (2008) Cyanoacetamide derivatives as synthons in heterocyclic synthesis. Turk J Chem 32(3):259–286
46. Metwally MA, Abdel-Latif E, Amer FA (2003) Synthesis and reactions of some thiocarbamoyl derivatives. Sulfur Lett 26(3):119–126. https://doi.org/10.1080/0278611031000095322
47. Iqbal Z, Wu WQ, Kuang DB, Wang L, Meier H, Cao D (2013) Phenothiazine-based dyes with bilateral extension of π-conjugation for efficient dye-sensitized solar cells. Dyes Pigments 96(3):722–731. https://doi.org/10.1016/j.dyepig.2012.11.010
48. Frisch MJ, Trucks GW, Schlegel HB, Scuseria GE, Robb MA, Cheeseman JR, Scalmani G, Barone V, Mennucci B, Petersson GA, Nakatsuji H, Caricato M, Li X, Hratchian HP, Izmaylov AF, Bloino J, Zheng G, Sonnenberg JL, Hada M, Ehara M, Toyota K, Fukuda R, Hasegawa J, Ishida M, Nakajima T, Honda Y, Kitao O, Nakai H, Vreven T, Montgomery JA Jr, Peralta JE, Ogliaro F, Bearpark M, Heyd JJ, Brothers E, Kudin KN, Staroverov VN, Kobayashi R, Normand J, Raghavachari K, Rendell A, Burant JC, Iyengar SS, Tomasi J, Cossi M, Rega N, Millam JM, Klene M, Knox JE, Cross JB, Bakken V, Adamo C, Jaramillo J, Gomperts R, Stratmann RE, Yazyev O, Austin AJ, Cammi R, Pomelli C, Ochterski JW, Martin RL, Morokuma K, Zakrzewski VG, Voth GA, Salvador P, Dannenberg JJ, Dapprich S, Daniels AD, Farkas Ö, Foresman JB, Ortiz JV, Cioslowski J, Fox DJ (2009) Gaussian 09. Gaussian, Inc., Wallingford
49. Nielsen AB, Holder AJ (2009) Gauss view 5.0, user's reference. GAUSSIAN Inc., Pittsburgh
50. Lee CT, Yang WT, Parr RG (1988) Development of the Colle-Salvetti correlation-energy formula into a functional of the electron density. Phys Rev B 37:785
51. Godbout N, Salahub DR, Andzelm J, Wimmer E (1992) Optimization of Gaussian-type basis-sets for local spin-density functional calculations. 1. Boron through neon, optimization technique and validation. Can. J. Chem. Rev. Can. Chim. 70:560–571
52. Neale NR, Kopidakis N, De Lagemaat JV, Gratzel M, Frank AJ (2005) Effect of a coadsorbent on the performance of dye-sensitized TiO_2 solar cells: shielding versus band-edge movement. J Phys Chem B 109(49):23183–23189. https://doi.org/10.1021/jp0538666
53. Ito S, Miura H, Uchida S, Takata M, Sumioka K, Liska P, Comte P, Pechy P, Gratzel M (2008) High-conversion-efficiency organic dye-sensitized solar cells with a novel indoline dye. Chem Commun 14:5194–5196. https://doi.org/10.1039/b809093a
54. El-Shafei A, Hussain M, Atiq A, Islam A, Han L (2012) A novel carbazole-based dye outperformed the benchmark dye N719 for high efficiency dye-sensitized solar cells (DSSCs). J Mater Chem 22(45):24048–24056. https://doi.org/10.1039/c2jm35267b

55. Lin RYY, Wu FL, Chang CH, Chou HH, Chuang TM, Chu TC, Hsu CY, Chen PW, Ho KC, Lo YH, Lin JT (2014) Y-shaped metal-free D-π-$(A)_2$ sensitizers for high-performance dye-sensitized solar cells. J Mater Chem A 2(9):3092–3101. https://doi.org/10.1039/c3ta14404f
56. Ying W, Guo F, Li J, Zhang Q, Wu W, Tian H, Hua J (2012) Series of new D-A-π-A organic broadly absorbing sensitizers containing isoindigo unit for highly efficient dye-sensitized solar cells. ACS Appl Mater Interfaces 4(8):4215–4224. https://doi.org/10.1021/am300925e
57. Oskam G, Bergeron BV, Meyer GJ, Searson PC (2001) Pseudohalogens for dye-sensitized TiO_2 photoelectrochemical cells. J Phys Chem B 105(29):6867–6873. https://doi.org/10.1021/jp004411d
58. Hua Y, Jin B, Wang H, Zhu X, Wu W, Cheung MS, Lin Z, Wong WY, Wong WK (2013) Bulky dendritic triarylamine-based organic dyes for efficient co-adsorbent-free dye-sensitized solar cells. J Power Sources 237:195–203. https://doi.org/10.1016/j.jpowsour.2013.03.018
59. Qu P, Meyer GJ (2001) Proton-controlled electron injection from molecular excited states to the empty states in nanocrystalline TiO_2. Langmuir 17(21):6720–6728. https://doi.org/10.1021/la010939d

Publisher's Note